Materials Today Communications 38 (2024) 107967

Contents lists available at ScienceDirect

Materials Today Communications

journal homepage: www.elsevier.com/locate/mtcomm

Investigating solid solutions: Geometric transformations triggered by germanium incorporation in $Cu_2ZnGe_xSn_{1-x}S_4$

Mohamed Issam Ziane [a,*], Moufdi Hadjab [b], Meftah Tablaoui [c], Hamza Bennacer [b,d], Mohammed Benali Kanoun [e], Souraya Goumri-Said [f,*]

[a] Laboratory of Electrical and Materials Engineering (LGEM), Higher School of Electrical and Energetic Engineering of Oran (ESGEEO), Algeria
[b] Department of Electronics, Faculty of Technology, University of M'sila, Algeria
[c] Research Center in Semiconductors Technologies for Energetic (CRTSE), Algiers, Algeria
[d] Elaboration and Physico-Mechanical and Metallurgical Characterization of Materials Laboratory (ECP3M), University of Mostaganem, Algeria
[e] Department of Mathematics and Sciences, College of Humanities and Sciences, Prince Sultan University, P.O. Box 66833, Riyadh 11586, Saudi Arabia
[f] Department of Physics, College of Science and General studies, Alfaisal University, P.O. Box 5092, Riyadh 11533, Saudi Arabia

ARTICLE INFO

Keywords:
CZGTS
DFT
Tetragonal-orthorhombic transition
Enthalpy of formation
Gibbs energy
Chalcogenides

ABSTRACT

Through experimental exploration, diverse phases—tetragonal and orthorhombic—have been observed within the $Cu_2ZnGe_xSn_{1-x}S_4$ region ($0 \leq x \leq 1$), hinting at potential miscibility gaps. To complement these findings, our computational investigation, employing density functional theory (DFT), delves into the Ge substitution-induced phase transition in $Cu_2ZnGe_xSn_{1-x}S_4$. Contrary to a single-phase behavior, our FP-LAPW at zero temperature results reveal a compelling shift from stannite (Sn-rich) to Wurtzite-Stannite (Ge-rich) at $x_{Ge} \approx 80\%$. Negative enthalpy of formation values indicates the inherent stability of these structures. The calculations reveal an estimated 8.884 meV per atom difference in enthalpies of formation between the Stannite and Wurtzite-Stannite phases for Cu_2ZnSnS_4. For Cu_2ZnGeS_4, the Wurtzite-Stannite structure emerges as the most stable, closely trailed by the Stannite structure, with enthalpies of formation at -4.833 eV·atom^{-1} and -4.804 eV·atom^{-1}, respectively. Furthermore, our quasi-harmonic Debye model facilitates the analysis of phase transitions triggered by the introduction of germanium. This is achieved by calculating the Gibbs energy, which remains unaffected by variations in temperature and pressure. As the tin cation is replaced by the smaller germanium cation, there is an observable decrease in the cell parameters. The corresponding reduction in cell volume adheres to the principles of Vegard's Law. Exploring the behavior of these materials in diverse conditions can significantly contribute to enhancing the performance and stability of devices built upon $Cu_2ZnGe_xSn_{1-x}S_4$.

1. Introduction

In the field of material science, the manipulation of intrinsic parameters, like alloy composition, and external conditions, such as temperature, pressure, or magnetic fields, allows the creation of novel materials with desired properties. Given the escalating demand for materials with specific attributes, computational methods for materials design has gained prominence. This is particularly evident due to the constraints of high costs and time associated with experimental discovery [1]. Computational methods, utilizing computer simulations in material science, play a pivotal role in predicting novel properties and designing materials with specific characteristics. These methods contribute valuable insights into the physical and chemical properties of systems that may be challenging or inaccessible through traditional means. Advancements in computer technology now enable the analysis of large and intricate systems. Among computational methods, density functional theory (DFT) stands out as a widely implemented tool in various codes for material science [2,3]. This potent technique employs electron density, rather than wave functions, to describe microscopic systems, offering a rapid and precise means of calculating diverse material properties, including energy, electronic structure, stability, phase transition, and other behaviors of interest. Notably, alloys based on chalcogenides have recently demonstrated considerable potential in enhancing the efficiency of solar cells. [4]. Furthermore, this class of material consists mostly of earth abundant and non-toxic elements [5] and can be manufactured using simple and low-cost processes [6].

* Corresponding authors.
E-mail addresses: issam1308@yahoo.fr (M.I. Ziane), sosaid@alfaisal.edu (S. Goumri-Said).

https://doi.org/10.1016/j.mtcomm.2023.107967
Received 3 November 2023; Received in revised form 21 December 2023; Accepted 23 December 2023
Available online 25 December 2023

Chalcogenide materials are useful for solar cells due to their unique optical and electrical properties, including high absorption coefficients and tunable bandgap energies [7]. Additionally, chalcogenides can be used to produce thin-film solar cells, which are lighter and more flexible than traditional silicon-based solar cells. Quaternary chalcogenide semiconductors are a type of chalcogenide material composed of four elements, usually including sulfur, selenium, tellurium, and one or more elements from groups 3 to 6 of the periodic table. Cu-based quaternary chalcogenide semiconductors (Cu_2-II-IV-VI_4) and derived alloys are a large type of material with great promise for a variety of applications, particularly as absorber layers in solar cell technologies [8,9]. An efficiency up to 12.6% has been achieved by Wang *et al.* in $Cu_2ZnSn(S_xSe_{1-x})_4$ based solar cells [10]. Additionally, several articles summarize results of research on the optimization of the material composition by partial cation substitutions revealed further increase in the efficiency. Indeed, due to its good miscibility the incorporation of Ge on Sn site in Cu_2ZnSnS_4 (CZTS) is quite promising and has recently gained much attention. It has been shown that a small doping with Ge in the $Cu_2ZnGe_xSn_{1-x}S_4$ solid solutions resulted in a real increase of the solar cell efficiency [11–14]. Accordingly, chalcogenide based alloys are extremely versatile materials, capable of crystallizing in a large variety of structures. For example, group Cu_2-II-IV-VI_4, perhaps the most studied group of this family. The cation rearrangement of this group of materials results in several possible phases. Stannite- or Kesterite-type structures that are the derivatives of sphalerite unit cells, by ordering the metals on the cation sites [15], and Wurtzite-Stannite or Wurtzite-Kesterite structures derived from the Wurtzite lattice based upon the valence octet rule. From the geometry of each phase, the stannite (I-42 m) and Kesterite (I-4) structures have Tetragonal symmetry, and an Orthorhombic for Wurtzite-Stannite (Pmn21) and Wurtzite-Kesterite (Pc) structures [16]. Additionally, a 'disordered Kesterite' phase (I-42 m) has been observed, in which the copper and zinc atoms in the 2c and 2d Wyckoff positions are randomly distributed [17].

The present paper has been motivated by an effort to elucidate the question of the phase transition induced by the incorporation of Ge atoms into the lattice of Cu_2ZnSnS_4 material. Phase transition in alloy plays an important role in many physical and chemical processes, and can greatly affect the properties and performance of materials. Understanding the structure change is crucial in fields such as materials science, thermodynamics, and engineering. In this study, we introduce computational methods for conducting resource-intensive ab initio computations to estimate these properties in Section 2. Subsequently, we delve into the results obtained for structural and thermodynamic properties in Section 3. Finally, we consolidate our findings and draw conclusions in Section 4.

2. Computational background

The calculations were performed using the (linearized) augmented plane-wave and local orbitals [(L)APW+lo] method to solve the Kohn-Sham equations of DFT [18]. The FP-LAPW+lo method is implemented in the famous WIEN2K package [19,20]. The code is an indispensable tool for the interpretation of experimental data as well as for the prediction of materials properties [21–24]. The revised Perdew-Burcke-Ernzerhof (PBEsol) parameterization of the generalized gradient approximation (GGA) functional [25] is used to describe the exchange and correlations (XC) effects for geometry optimization. The calculations of the structural properties and enthalpy of formation were based on the fully relaxed cells. The muffin-tin sphere radius R_{mt} was chosen as 2.00, 2.10, 2.10, 2.25, and 1.80 a.u radii, respectively, for Cu, Zn, Ge, Sn, and S. $R_{mt}K_{max}$ parameters that determines matrix size for convergence is fixed for 7. As convergence conditions, 10^{-8} Rydberg for the total energy was used in almost all calculations. In order to obtain a more accurate representation of the electronic properties of the material, the integration over the irreducible part of Brillouin zone is carried out on a grid of $3 \times 4 \times 5$ k points.

3. Results and discussion

In this study we expand our efforts to explore the structural phases in the Ge element substituting process along the $Cu_2ZnGe_xSn_{1-x}S_4$ solid solution (x = 0–1), investigating both tetragonal (stannite) and orthorhombic (wurtzite-stannite) symmetry. From experimental observations, resting on the X-ray diffraction analysis, Nagaoka *et al.* confirmed that Cu_2ZnSnS_4 belonged to an ordered tetragonal stannite structure with the space group of I-42 m [26,27]. The stannite (St) phase can be derived from a doubled zincblende crystal structure by two particular pairwise cation substitutions [28,29]. This stannite structure is composed of alternating layers of mixed Zn and Sn cations which are separated by layers of Cu ions. There are four non-equivalent Wyckoff positions (WP): Zn divalent cation occupies the origin 2a (0, 0, 0), Cu monovalent cation at the 4d (0, 1/2, 1/4), Sn at the 2b site (0, 0, 1/2), and the S anion located at 8i (1/4, 1/4, 1/8). Even more, CZTS have also been shown to exist in other phases such as wurtzite-stannite (WS) with a hexagonal crystal cell [30,31]. In the wurtzite superstructure of the Pmn21 space group (No. 31), there are three S atoms occupying Wyckoff positions at 4b (0.2245, 0.1617, 0.1191), 2a (0, 0.2956, 0.664), and 2a (0, 0.6352, 0.0872), one Cu at 4b (0.2252, 0.1761, 0.4836) while Zn and Ge atoms are located at 2a (0, 0.6521, 0.4909) and 2a (0, 0.3192, 0) sites, respectively [32]. The presence of Cu_2ZnGeS_4, herein referred to as CZGS, has been ascertained to adopt the Stannite-type structure by Doverspike *et al.* [33] and Chen *et al.* [34] through meticulous examination utilizing Raman spectroscopy and X-ray diffraction techniques. Moreover, Levcenco *et al.* [35], employing powder X-ray diffraction in combination with Rietveld refinement, have further corroborated the existence of the CZGS system in an orthorhombic structure, specifically identified as wurtzite-stannite (space group: Pmn21). In this structure, the three elements Cu, Zn, Ge/Sn in quaternary sulfides Cu_2ZnXS_4 (X = Ge, Sn) are tetrahedrally surrounded by S and each S is surrounded by one Zn, one Ge/Sn and two Cu atoms (Fig. 1). In analogy to stannite cell, the wurtzite-stannite is also acentric structure and the cationic elements coordination around each S atom as in stannite structure.

In the present work, the supercell for tetragonal stannite system was replicated $2 \times 2 \times 2$, containing 64 atoms in the $Cu_2ZnGe_xSn_{1-x}S_4$ primitive structure. For wurtzite-stannite, a unit cell consisting of four Cu_2ZnSnS_4 units, namely a $2 \times 2 \times 1$ supercell was used to build the $Cu_2ZnGe_xSn_{1-x}S_4$ systems. So, for all alloys in both phases, a 64 atoms based supercells with different random arrangements of Ge and Sn are constructed. Here, it is important to note that our constructed supercells for stannite/wurtzite-stannite structures consist of three possible substitutions (x = 0.25, 0.5 and 0.75) in which Ge and Sn cations are randomly distributed in the lattice. Nonetheless, the ability to explore compositions is restricted by the computational expense. When dealing with smaller compositions, it becomes necessary to utilize excessively large supercells (i.e., containing a large number of atoms), resulting in a significant escalation in computational costs. Additionally, a supercell was generated for three atomic positions of substitution atoms (Ge and Sn) in which one atom had a multiplicity of four, and two atoms had a multiplicity of two. This means that for each Ge composition in the $Cu_2ZnGe_xSn_{1-x}S_4$ solid solution, two different cation arrangements (Ge and Sn) are possible.

To attain this objective, it is essential to identify the most stable configuration by calculating the enthalpy of mixing (indicating the miscibility of the alloys) through FP-LAPW for each Ge composition. This involves assessing the enthalpies at various points between the minimum energies for each configuration and incorporating the mixing energies derived from the pure quaternary compounds, considering both the initial and final compositions (x = 0 and 1).

$$\Delta H = E_{CZGTS}^{\min} - E_{CZGTS}^{mix} \quad (1)$$

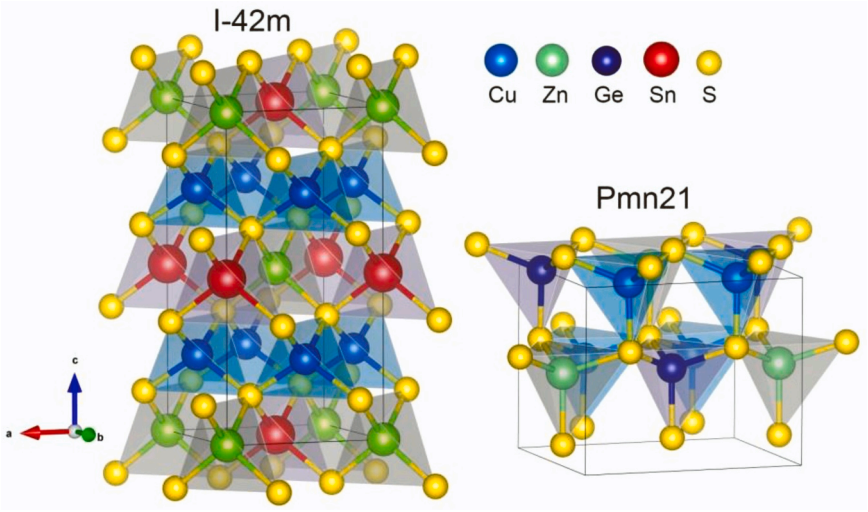

Fig. 1. Three-dimensional polyhedral view of the Cu_2ZnSnS_4 stannite (tetragonal I-42 m) and Cu_2ZnGeS_4 wurtzite-stannite (orthorhombic Pmn21) unit cells. The crystal structure figures are prepared using VESTA [36].

E^{mix}_{CZGTS} corresponds to the mixing energy and E^{min}_{CZGTS} is the equilibrium GGA-PBEsol calculated total energies of $Cu_2ZnGe_xSn_{1-x}S_4$ at 0 K. The mixing energy for the quinary alloys with different Ge compositions can be calculated from the pure quaternary energies by

$$E^{mix}_{CZGTS} = x.E^{min}_{CZGS} + (1-x)E^{min}_{CZTS} \quad (2)$$

E^{min}_{CZTS} and E^{min}_{CZGS} are the minimum energies obtained within GGA-PBEsol for pure quaternary alloys CZTS and CZGS, respectively.

Determining the most stable configuration hinges on evaluating the energy difference, where the configuration boasting the lowest enthalpy of mixing (or minimum energy) is recognized as the most stable. However, it is crucial to establish an initial reference point, specifically the favorable supercell configuration corresponding to the provided composition. In Figs. 2 and 3, the mixing enthalpies for $Cu_2ZnGe_xSn_{1-x}S_4$ alloys are presented, specifically focusing on zero temperature calculations for both crystalline phases. Traditionally, the formation enthalpy of most alloys can be approximated as a quadratic function of the composition x [37]. Closed symbols in Figs. 2 and 3 denote configurations with lower mixing enthalpies. In the case of the stannite phase, calculations for the two configurations exhibit significant overlap, with marginal differences of 0.408, 1.224, and 0.817 μeV observed for x = 25%, 50%, and 75%, respectively. The variation in mixing enthalpies follows a non-linear variation, characterized by the bowing parameter b (interaction parameter), determined through fitting this non-linear trend of mixing enthalpies to specific Eqs. (3) and (4), respectively for the stannite (St) and wurtzite-stannite (WS) phases. The quadratic term is contingent on the bowing parameter b.

$$\Delta H^{St} = -0.00743 + 2.23775x - 2.22936x^2 \quad (3)$$

$$\Delta H^{WS} = 0.03804 + 0.7439x - 0.8377x^2 \quad (4)$$

The interaction parameter 'b' serving as an indicative measure of alloy solubility is predicted to be − 2.22 eV for the stannite structure and − 0.83 eV for the wurtzite-stannite structure. The smaller bowing

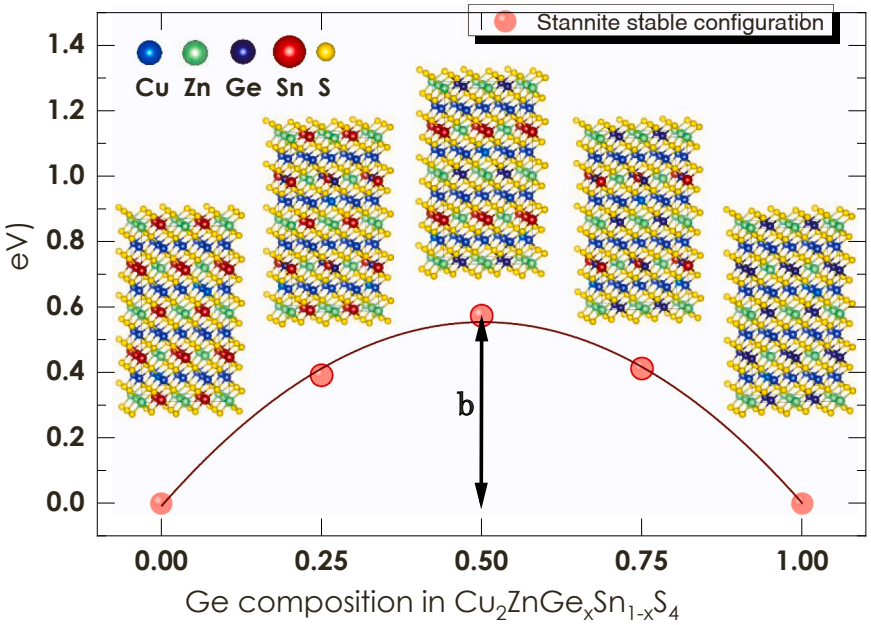

Fig. 2. Mixing enthalpies (ΔH) for different Ge compositions (x) of $Cu_2ZnGe_xSn_{1-x}S_4$ alloys in the stannite supercell, given in eV and per formula unit. The closed circles indicate the lowest energy configuration. The Fig. 2 also displays the crystalline configurations with the lowest mixing enthalpy.

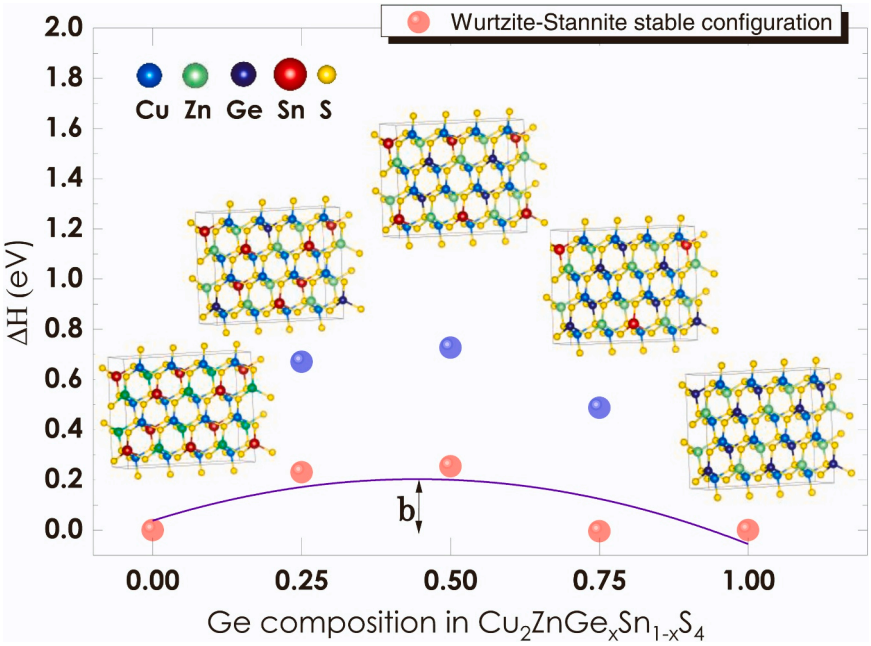

Fig. 3. Mixing enthalpies (ΔH) given in eV and per formula unit of wurtzite-stannite supercell at different Ge compositions (x). The closed square symbols are for the lowest energy configuration. The crystalline configurations with lowest mixing enthalpy are presented.

parameter observed for wurtzite-stannite, compared to stannite, suggests that component-uniform $Cu_2ZnGe_xSn_{1-x}S_4$ alloys can be more readily grown in the wurtzite-stannite structure than in the Stannite structure under standard growth temperature conditions.

As previously mentioned, this study unveils a substitution-induced phase transition in $Cu_2ZnGe_xSn_{1-x}S_4$ solid solutions at an intermediate x composition. This is accomplished through an extensive FP-LAPW calculation of mixing enthalpies of formation for both the stannite and wurtzite-stannite structures, covering molar fractions from $x = 0$ to $x = 1$. Anticipated in this process is the occurrence of a transition between the two phases. To determine the ground state structure, a comprehensive structural relaxation of all atoms in the supercell is carried out, while maintaining a fixed unit cell volume. These structural relaxations serve to compute the structural and thermodynamic properties of the ground state structures.

Thermodynamically, a phase transition or phase transformation signifies the alteration or conversion of a substance's phase from one thermodynamic state to another. The thermodynamic state of a system is defined by Gibbs energy (G), entropy (S), or enthalpy (H), which function based on one or more variables, usually temperature (T), pressure (P), and composition or molar fraction (x) in the context of an alloy. Several studies have focused on predicting the heat of formation, also known as enthalpy of formation, as it is a crucial parameter in thermodynamic modeling. This parameter plays a key role in various applications, including the calculation of phase diagrams [38]. The enthalpy term significantly influences the phase formation and stability of a multicomponent alloy. The mixing enthalpy of formation, also referred to as the enthalpy of mixing, quantifies the heat released or absorbed during the combination of two or more substances to create a solution. This parameter is closely tied to a chemical contribution, which considers the impact of electron redistribution during the formation of the alloy [39]. The mixing enthalpy of formation is determined by calculating the disparity between the enthalpy of the final mixture and the sum of the enthalpies of the individual components in their pure states. A negative mixing enthalpy implies greater stability in the mixed alloy structure compared to the individual structures, while a positive mixing enthalpy indicates that the individual structures are more stable than the mixed alloy structure.

Here, the mixing enthalpy of formation ΔH_{mix} is calculated per atom both in tetragonal (I-42 m) and orthorhombic (Pmn21) phases for $Cu_2ZnGe_xSn_{1-x}S_4$ alloys by subtracting the minimal total energy of the CZGTS in the equilibrium crystal structure from the sum of mixing energies of pure constituent elements in their ground states at the same temperature and pressure as the solid solution with respect to molar fractions of x in the solid solution. The mixing enthalpy of formation ΔH_{mix} is calculated by means of Eq. (5).

$$\Delta H_{mix}(Cu_2ZnGe_xSn_{1-x}S_4) = \left[\left(E^{\min}_{Cu_2ZnGe_xSn_{1-x}S_4}\right) - \sum\left(2E^{\min}_{Cu} + E^{\min}_{Zn} + xE^{\min}_{Ge} + (1-x)E^{\min}_{Sn} + 4E^{\min}_{S}\right)\right]\Big/ n \quad (5)$$

Here, n represents the number of atoms in the unit cell. It is worth noting that all minimum total energies are calculated at 0 K and 0 Pa and obtained with the same XC functional, $R_{mt}K_{max}$ and K points parameters for both tetragonal (I-42 m) and orthorhombic (Pmn21) phases.

The Figs. 4 and 5 show the calculation results for ΔH in the stannite

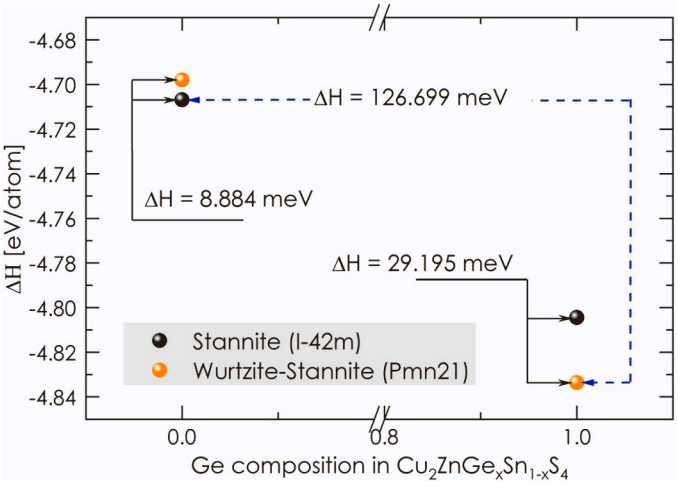

Fig. 4. Calculated enthalpies of formation (ΔH) at 0 K for Cu_2ZnSnS_4 and Cu_2ZnGeS_4 in stannite, and wurtzite-stannite structures.

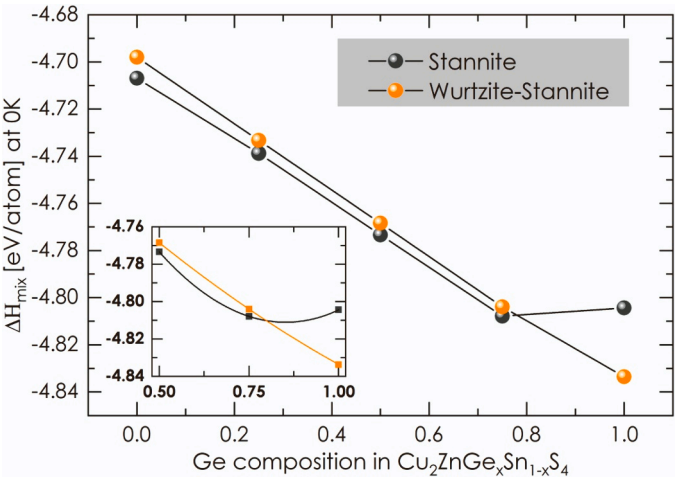

Fig. 5. The dependence of the mixing enthalpies of formation at 0 K showing potential Ge composition-induced transition in the $Cu_2ZnGe_xSn_{1-x}S_4$ solid solution. The inset plot the polynomial fit of the mixing enthalpies from x = 0.5 to 1.

and wurtzite-stannite phases for Cu_2ZnSnS_4 and Cu_2ZnGeS_4 compounds, as well as the variation of ΔH_{mix} as a function of the Ge composition for the $Cu_2ZnGe_xSn_{1-x}S_4$ solid solution alloy, respectively. A second-order polynomial was used to generate a fit of ΔH_{mix} versus the x composition, which was found to be an acceptable fit. The significance of ΔH_{mix} in determining the phase formation of solid solution alloys is evident. Furthermore, a negative value of ΔH_{mix} indicates the release of energy upon mixing, which signifies an exothermic process. This suggests that the formation of all alloys is a thermodynamically favorable process.

From Fig. 4 it is clear that the enthalpies of formation for stannite and wurtzite-stannite structures of Cu_2ZnSnS_4 and Cu_2ZnGeS_4 compounds are close in value. Our DFT calculations show that the stannite structure represents the ground state configuration of the Cu_2ZnSnS_4 ($x_{Ge} = 0\%$) system when compared to the wurtzite-stannite structure. The calculations indicate that the difference in enthalpies of formation (ΔH) between the stannite and wurtzite-stannite phases for CZTS is estimated to be 8.884 meV per atom. In comparison to other theoretical results, our estimation differs from Saini *et al.* [12] by + 3.484 meV per atom and from Maeda et al. [40] by − 46.116 meV per atom. Additionally, our calculations demonstrate a lower formation enthalpy for the Cu_2ZnSnS_4 system compared to the estimation suggested by Maeda *et al.* Specifically, the present results for both stannite and wurtzite-stannite phases are − 4.706 eV/atom and − 4.698 eV/atom, respectively, in contrast to Maeda *et al.'s* values of − 3.7301 eV/atom and − 3.6751 eV/atom. These discrepancies amount to underestimations of 26.162% and 27.830%, respectively, for the stannite and wurtzite-stannite phases when compared to Maeda et al.'s values. It is worth noting that the enthalpy of formation of a solid solution can depend on the specific conditions under which it is formed, such as temperature and pressure, as well as the experimental preparation method. Similarly, in theoretical predictions, calculation methods rely on mathematical and physical models that frequently incorporate approximations, some of which necessitate the input of experimental parameters. As a result, the calculated enthalpy of formation may not always align with both the experimental and theoretically predicted values.

For Cu_2ZnGeS_4 compound, the wurtzite-stannite is the most stable structure, closely followed by stannite, with enthalpies of formation of $-4.833\ eV{\cdot}atom^{-1}$ and $-4804\ eV{\cdot}atom^{-1}$, respectively. The literature does not contain any concrete reports on enthalpy studies for Cu_2ZnGeS_4 system. Moreover, our DFT studies indicate that the energy difference between the stannite and wurtzite-stannite phases in CZTS is smaller than that in CZGS amounting to 29.195 eV per atom.

Fig. 5 illustrates the relationship between the composition of germanium and the mixing enthalpies at 0 K in both phases of the $Cu_2ZnGe_xSn_{1-x}S_4$ system. The increase in the ionic radius of the cation from germanium to tin leads to a rise in the relative ionic potential and, as a result, an increase in the absolute value of the mixing enthalpy [41]. Moreover, the Fig. 5 shows that as the germanium content increases, the mixing enthalpy of formation decreases. It is also indicated that the tetragonal stannite phase remains stable up to around 80% germanium content within CZGTS. After surpassing this threshold, a shift in phase occurs. This shift is driven by a decrease in the mixing enthalpy of formation for the orthorhombic wurtzite-stannite structure relative to the tetragonal stannite structure. Consequently, even a small amount of Sn renders the CZTGS unstable in the stannite configuration, prompting a transformation into a WS-like phase at x values greater than 80%. The alloys in the stannite phase exhibit a stronger alloying ability compared to those in the wurtzite-stannite phase when the Ge content is below 80%. The calculated bowing parameter 'b′ for the mixing formation energy of wurtzite-stannite phase is only + 0.012 eV/atom, compared to + 0.080 eV/atom in the stannite phase, indicating good miscibility of Ge and Sn in the WS phase. The results of the interaction parameters 'b′ showing the mixing of the Sn and Ge cations is strongly influenced by the specific cation ordering in the crystalline structure. Upon examining Fig. 5, it is evident that the enthalpy energy of mixing for both structures follows a linear trend up to approximately x = 0.75. However, beyond this point, the stannite phase exhibits a significant curvature, suggesting potential instability for higher concentrations of Ge in the $Cu_2ZnGe_xSn_{1-x}S_4$ alloy. Furthermore, the energy disparities between stannite and wurtzite-stannite alloys remain remarkably minimal, with values not surpassing 8 meV per atom up to x = 0.75. This suggests the potential for both the stannite and wurtzite-stannite phases to coexist under the standard growth temperature. As mentioned earlier, a shift from the stannite phase to the wurtzite-stannite phase takes place at approximately $x_{Ge} \approx 80\%$. At this specific composition, the system can be considered an ideal mixing case with a ΔH_{mix} of zero, and the solid-solution phase is expected to be stabilized with a more negative ΔH_{mix}.

To comprehend the structural phase transition from stannite to wurtzite-stannite induced by the introduction of germanium to the CZTS compound, an analysis of the Gibbs energy at different temperatures was imperative. Gibbs energy plays a pivotal role in elucidating phase transitions as it quantifies the free energy accessible for productive work resulting from volume variations. In this investigation, free Gibbs energies were forecasted using the quasi-harmonic Debye mode across temperatures spanning from 0 to 1000 K. The non-equilibrium Gibbs free energy function was expressed using the following equation:

$$G^*(V;p,T) = E(V) + pV + F^*_{vib}\big(\Theta(V);T\big) = F^*\big(\Theta(V);T\big) + pV \quad (6)$$

Here, E (V), pV are respectively, the total energy, the constant hydrostatic pressure condition. F_{vib} is the vibrational Helmholtz free energy which includes both the vibrational contribution to the internal energy and the entropy S that are strong functions of temperature and Θ (V) is the Debye temperature. When the pressure and temperature are both at zero, the Gibbs energy of a system is equivalent to the enthalpy H, which represents the system's energy.

Fig. 6 illustrates the variation in mixing enthalpy of formation and Gibbs free energy between the stannite and wurtzite-stannite phases across different x compositions, under zero-pressure conditions. The transition from stannite to wurtzite-stannite in the CZTS structure becomes apparent beyond 0.75, approximately at the 80% Ge composition. This observation aligns with the findings obtained from assessments of mixing enthalpies of formation conducted at absolute zero temperature (0 K) and zero pressure (0 P). Fig. 6 demonstrates a striking similarity between the Gibbs energy calculation and the mixing enthalpy of formation.

Fig. 7 illustrates the temperature-dependent Gibbs energy difference (G_{St}-G_{WS}) across various x compositions, excluding any influence from

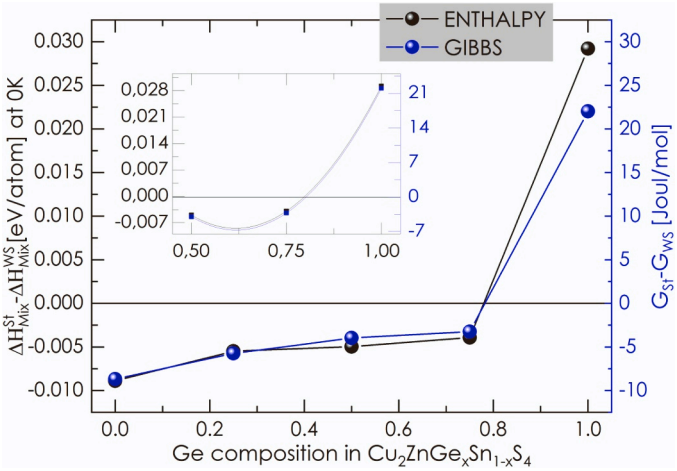

Fig. 6. Variation in the discrepancy between the mixing enthalpy of formation (black) and Gibbs free energy (blue) values obtained for the stannite phase compared to the wurtzite-stannite phase is contingent upon the germanium composition within CZGTS. The inset plot the polynomial fit of the mixing enthalpies and Gibbs energy from 0.5 to 1.

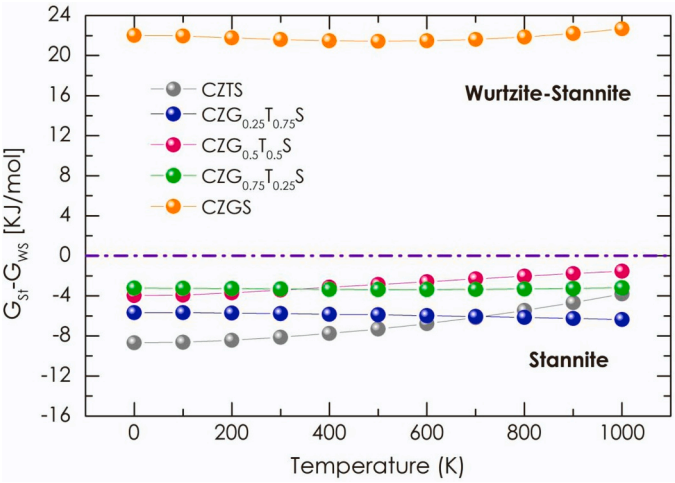

Fig. 7. Temperature dependence of Gibbs energy difference (G_{St}-G_{WS}) across a range of x compositions excluding any effects resulting from pressure.

pressure effects. It is crucial to recognize that, for quaternary compounds and quinary alloys with compositions ranging from 0.25 to 0.75, the thermodynamic difference in Gibbs free energy remains largely unaffected by temperature. This implies that the capacity of these quinary alloys to modify their crystalline structure is not strongly influenced by thermal energy, as anticipated by the Gibbs2 code [42]. The materials in question maintain their structures consistently across all temperature ranges.

As observed in the calculation of Gibbs energy as a function of temperature, a similar lack of substantial impact is noted when considering pressure variations in Fig. 8. The assessment of pressure effects on the Gibbs energy difference reveals minimal influence up to 16 GPa for almost all x compositions. The calculations emphasize that the phase transition is primarily driven by the composition of germanium in $Cu_2ZnGe_xSn_{1-x}S_4$, with pressure exerting a very limited effect on the observed transition.

The optimization process for lattice parameters begins by utilizing the experimentally determined volume of pure quaternary compounds, CZTS and CZGS. However, for quinary alloys where experimental values are unavailable, optimization is carried out by estimating lattice

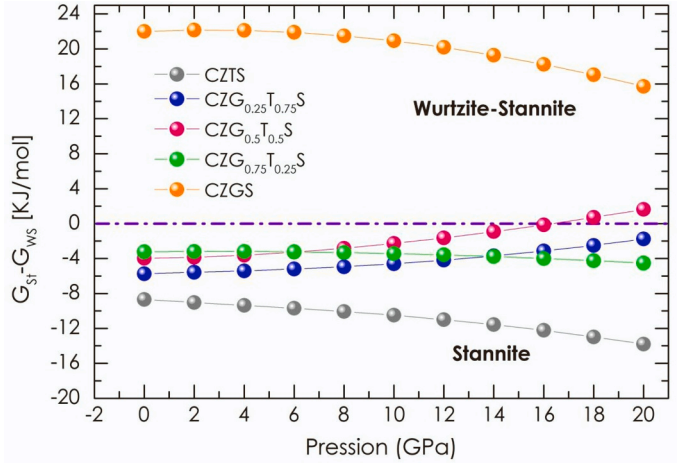

Fig. 8. Pressure dependence of Gibbs energy difference (G_{St}-G_{WS}) across different x compositions, while maintaining a constant temperature at 0 K.

parameters through Vegard's law. In this scenario, the DFT method, specifically the GGA-PBEsol approximation, is employed to calculate the ground-state energy E (V) for both stannite and wurtzite-stannite structures, with the unit cell volume V serving as the variable parameter. The properties of $Cu_2ZnGe_xSn_{1-x}S_4$ solid solution alloys were determined by fitting the calculated energy E (V) to the Murnaghan equation of state concerning both volume and pressure. The obtained results, along with the experimental values for quaternary compounds, are presented in Table 1.

It is noteworthy that the crystal lattice parameters derived from the calculations presented in Table 1 are in agreement with the experimental values reported previously for pure quaternary compounds.

Fig. 9. illustrates the relationships between the parameters of $Cu_2ZnGe_xSn_{1-x}S_4$ solid solutions and their composition. In this figure, the scattered points correspond to the calculated values of lattices parameters and volumes at various Ge compositions. It is evident from the graph that the Ge element incorporation in CZTS causes the unit cell to shrink, by a decrease in the lattice parameters, which is well consistent with other experimental report [43–45]. The varying composition of $Cu_2ZnGe_xSn_{1-x}S_4$ solid solutions causes non-uniform changes in the lattice parameters for stannite structures, reflecting the complex interplay between the constituent elements. In general, the lattice parameter variation trend of $Cu_2ZnGe_xSn_{1-x}S_4$ with Ge composition can be described by

$$x \leq 0.80 \Rightarrow \begin{cases} a = 5.3865 - 0.1714x + 0.0872x^2 \\ c = 10.7582 - 0.0237x - 0.2997x^2 \end{cases} \quad (7)$$

$$x \geq 0.80 \Rightarrow \begin{cases} a = 7.7570 - 0.3524x + 0.0305x^2 \\ b = 6.4769 + 0.0004x - 0.0556x^2 \\ c = 6.2168 - 0.1345x + 0.0472x^2 \end{cases} \quad (8)$$

As illustrated in Fig. 9 and apparent from Eqs. (7) and (8), the bowing parameter *b* determined through a fitting of the nonlinear trend in the calculated lattice parameters, is more noticeable in the stannite phase than in the wurtzite-stannite phase. Specifically, in the stannite region, lattice parameter *a* deviates slightly negatively by + 0.0872 Å from Vegard's law, while the lattice parameter *c* exhibits a considerably larger positive deviation with a value of − 0.2997 Å. Conversely, when the Ge content exceeds 80%, within the wurtzite-stannite region, a small deviation is observed for lattice parameters, not exceeding 0.055 Å. Furthermore, in Fig. 9, it is observed that the decrease in cell volume with the increase of Ge content follows Vegard's law for the $Cu_2ZnGe_xSn_{1-x}S_4$ solid solutions. In both crystalline phases, there is a linear decrease in cell volume as the composition varies from x = 0 to x = 1. At x = 0.80, the orthorhombic WS phase exhibits a slightly lower

Table 1
Optimized primitive cell volume, lattices parameters (*a*), (b) and (c), the (c/a) and (b/a) ratio, bulk modulus (*B*) at ground state conditions for both stannite and wurtzite-stannite structures.

Ge compositions	*Space group*	a (Å)	b (Å)	c (Å)	b/a	c/a	B (GPa)
Cu_2ZnSnS_4							
GGA-PBEsol	*I-42m*	5.3836	-	10.7673	-	1.9999	82.4666
	Pmn21	7.7572	6.4757	6.2174	0.8348	0.8015	80.8786
Exp. results	*I-42m*	**5.430**[a]	-	**10.830**[a]	-	**1.9944**[a]	-
	Pmn21	**7.9736**[b]	**6.6116**[b]	**6.2908**[b]	**0.8291**[b]	**0.7812**[b]	-
$Cu_2ZnGe_{0.25}Sn_{0.75}S_4$							
GGA-PBEsol	*I-42m*	5.3536	-	10.7200	-	2.0024	83. 5466
	Pmn21	7.6703	6.4760	6.1853	0.8443	0.8064	83.7673
Exp. results	*I-42m*	-	-	-	-	-	-
	Pmn21	-	-	-	-	-	-
$Cu_2ZnGe_{0.5}Sn_{0.5}S_4$							
GGA-PBEsol	*I-42m*	5.3264	-	10.6583	-	2.0010	86.3748
	Pmn21	7.5905	6.4648	6.1619	0.8517	0.8118	83.4194
Exp. results	*I-42m*	-	-	-	-	-	-
	Pmn21	-	-	-	-	-	-
$Cu_2ZnGe_{0.75}Sn_{0.25}S_4$							
GGA-PBEsol							
	I-42m	5.2973	-	10.6031	-	2.0016	85.7387
	Pmn21	7.5092	6.4429	6.1440	0.8580	0.8182	86.4676
Exp. results	*I-42m*	-	-	-	-	-	-
	Pmn21	-	-	-	-	-	-
Cu_2ZnGeS_4							
GGA-PBEsol	*I-42m*	5.3064	-	10.4214	-	1.9639	84.7781
	Pmn21	7.4353	6.4233	6.1289	0.8639	0.8243	88.6538
Exp. results	*I-42m*	**5.342**[c]	-	**10.516**[c]	-	**1.9685**[c]	-
	Pmn21	**7.509**[c]	**6.479**[c]	**6.192**[c]	**0.8628**[c]	**0.8246**[c]	-

[a] Ref. [26] [b] Ref. [30] [c] Ref. [43]

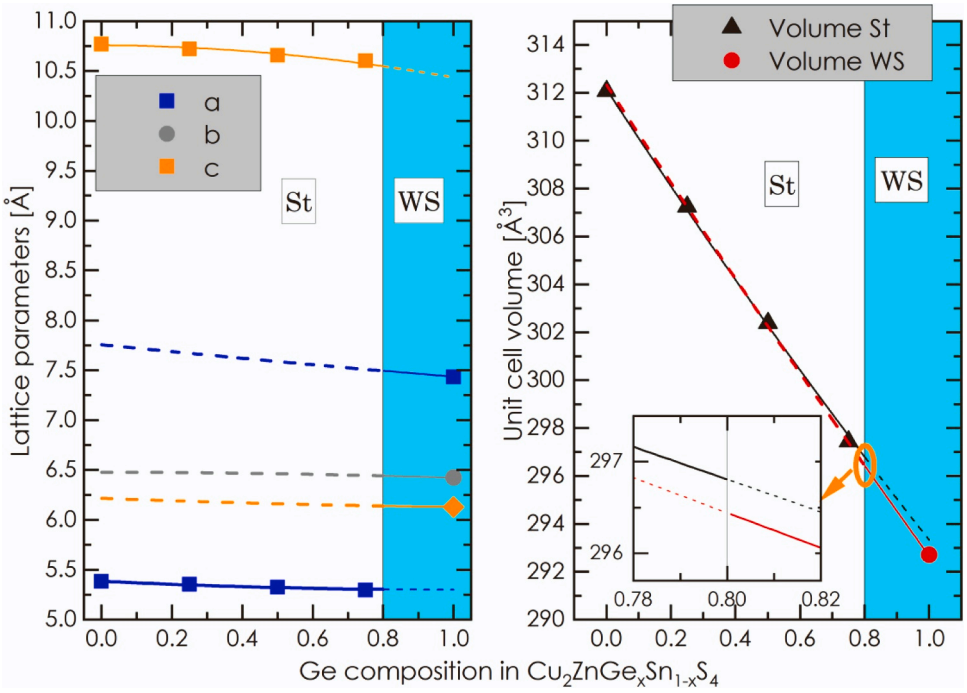

Fig. 9. Lattice parameters and volume as x composition of $Cu_2ZnGe_xSn_{1-x}S_4$ alloys for both stannite and wurtzite-stannite structures.

cell volume than the tetragonal St phase. However, beyond this value, the calculated volume of the tetragonal St phase surpasses that of the orthorhombic (WS) phase. This difference in cell volume between the orthorhombic and tetragonal phases may favor a transformation from the stannite phase to the wurtzite-stannite phase under certain conditions.

4. Conclusion

Our investigations delved into the phase changes induced by the substitution of Sn with Ge in Cu_2ZnSnS_4 and its impact on structural properties. Utilizing the WIEN2K computational code, we systematically examined the enthalpy's role in the phase stability and formation of $Cu_2ZnGe_xSn_{1-x}S_4$ (x = 0–1.0). Our findings align with the typical behavior of Cu_2-II-IV-S_4 tetrahedral quaternary chalcogenides, exhibiting the stannite structure with Sn and the wurtzite-stannite structure

with Ge. Specifically, our calculations indicate that higher Ge content stabilizes the wurtzite-stannite structure, while higher Sn content stabilizes the Stannite structure at zero temperature. The dominance of the IV element size dictates the stacking of sulfur atoms, resulting in orthorhombic structure with germanium and tetragonal structure with tin. Germanium can be substituted for tin up to ≈ 80% in the tetragonal stannite structure of $Cu_2ZnGe_xSn_{1-x}S_4$, as predicted at zero temperature. Notably, the Gibbs energy analysis reveals that the transition is independent of temperature, and the calculations indicate no significant variation in the Gibbs free energy obtained from the tetragonal or orthorhombic structures.

Acknowledgments

Authors from Algeria are grateful to the General Directorate for Scientific Research and Technological Development (DGRSDT) of Algeria. This work falls under the PRFU research project N°: A10N01UN280120220006. The author (MBK) would like to thank Prince Sultan University for their support.

CRediT authorship contribution statement

M. I. Ziane: Conceptualization. M. I. Ziane, M. Hadjab, M. Tablaoui, H. Bennacer, M. B. Kanoun, S. Goumri-Said: Methodology, Software, Data curation, Writing – original draft, Visualization, Investigation. M. I. Ziane, S. Goumri-Said: Supervision. M. I. Ziane, M. Hadjab, M. Tablaoui, H. Bennacer, M. B. Kanoun, S. Goumri-Said: Writing – review & editing.

Declaration of Competing Interest

The authors declare that they have no known competing financial interests or personal relationships that could have appeared to influence the work reported in this paper.

Data Availability

No data was used for the research described in the article.

References

[1] J.J. Low, N.H. Paulson, M. D'Mello, M. Stan, Thermodynamics of monoclinic and tetragonal hafnium dioxide (HfO_2) at ambient pressure, CALPHAD: Comput. Coupling Phase Diagr. Thermochem. 72 (2021), 102210.
[2] B. Amin, I. Ahmad, M. Maqbool, S. Goumri-Said, R. Ahmad, Ab initio study of the bandgap engineering of $Al_{1-x}Ga_xN$ for optoelectronic applications, J. Appl. Phys. 109 (2) (2011), 023109.
[3] M.B. Kanoun, S. Goumri-Said, A.E. Merad, H. Mariette, Ab initio study of structural parameters and gap bowing in zinc-blende $Al_xGa_{1-x}N$ and $Al_xIn_{1-x}N$ alloys, J. Appl. Phys. 98 (6) (2005), 063710.
[4] C.J. Bosson, M.T. Birch, D.P. Halliday, K.S. Knight, A.S. Gibbs, P.D. Hatton, Cation disorder and phase transitions in the structurally complex solar cell material Cu_2ZnSnS_4, J. Mater. Chem. A 5 (2017) 16672.
[5] M.I. Ziane, H. Bennacer, M. Mostefaoui, M. Tablaoui, M. Hadjab, A. Saim, K. Bekhedda, Anisotropic optical properties of $Cu_2ZnSn(S_xSe_{1-x})_4$ solid solutions, Opt. Int. J. Light Electron Opt. 243 (2021), 167490.
[6] D. Fritsch, S. Schorr, On the ground state crystal structure of $(Ag_{0.5}Cu_{0.5})2ZnSnSe_4$, Thin Solid Films 738 (2021) 138957.
[7] R. Woods-Robinson, Y. Han, H. Zhang, T. Ablekim, I. Khan, K.A. Persson, A. Zakutayev, Wide band gap chalcogenide semiconductors, Chem. Rev. 120 (9) (2020) 4007–4055.
[8] Nautiyal, H., Lohani, K., Mukherjee, B., Isotta, E., Malagutti, M.A., Ataollahi, N., Pallecchi, I., Putti, M., Misture, S.T., Rebuffi, L., & Scardi, P. (2023). Mechanochemical Synthesis of Sustainable Ternary and Quaternary Nanostructured Cu2SnS3, Cu2ZnSnS4, and Cu2ZnSnSe4 Chalcogenides for Thermoelectric Applications. Nanomaterials, 13, 366.
[9] M. Dimitrievska, F. Boero, A.P. Litvinchuk, S. Delsante, G. Borzone, A. Perez-Rodrigue, V. Izquierdo-Roca, Structural polymorphism in "Kesterite " Cu_2ZnSnS_4: Raman spectroscopy and first-principles calculations analysis, Inorg. Chem. 56 (6) (2017) 3467–3474.
[10] W. Wang, M.T. Winkler, O. Gunawan, T. Gokmen, T.K. Todorov, Y. Zhu, D.B. Mitzi, Device characteristics of CZTSSe thin-film solar cells with 12.6% efficiency, Adv. Energy Mater. 4 (7) (2013) 1301465.
[11] Q. Guo, G.M. Ford, W.-C. Yang, C.J. Hages, H.W. Hillhouse, R. Agrawal, Enhancing the performance of CZTSSe solar cells with Ge alloying, Sol. Energy Mater. Sol. Cells 105 (2012) 132–136.
[12] I. Kim, K. Kim, Y. Oh, K. Woo, G. Cao, S. Jeong, J. Moon, Band gap-graded $Cu_2Zn(Sn_{1-x}Ge_x)S_4$ thin-film solar cells derived from metal chalcogenide complex ligand capped nanocrystals, Chem. Mater. 26 (13) (2014) 3957–3965.
[13] C.J. Hages, S. Levcenco, C.K. Miskin, J.H. Alsmeier, D. Abou-Ras, R.G. Wilks, R. Agrawal, Improved performance of Ge-alloyed CZTGeSSe thin-film solar cells through control of elemental losses, Prog. Photovolt.: Res. Appl. 23 (3) (2013) 376–384.
[14] N. Saini, J.K. Larsen, K. Lindgren, A. Fazi, C. Platzer-Björkman, Band gap engineered $Cu_2ZnGe_xSn_{1-x}S_4$ solar cells using an adhesive TiN back contact layer, J. Alloy. Compd. 880 (2021), 160478.
[15] R. Chetty, A. Bali, O.E. Femi, K. Chattopadhyay, R.C. Mallik, Thermoelectric properties of in-doped $Cu_2ZnGeSe_4$, J. Elect. Mat. 45 (3) (2016) 1625–1632.
[16] W. Shi, A.R. Khabibullin, L.M. Woods, Exploring phase stability and properties of I-II2-III-VI4 quaternary chalcogenides, Adv. Theory Simul. 3 (1) (2020), 2000041.
[17] A. Khelfane, M.I. Ziane, M. Tablaoui, M. Hecini, D. Ouadjaout, M. Derbal, Composition dependence of the optical band gap and the secondary phases via zinc content in CZTS material, Inorg. Chem. Commun. 151 (2023), 110639.
[18] W. Kohn, L.J. Sham, Self-consistent equations including exchange and correlation effects, Phys. Rev. A. Gen. Phys. 140 (4A) (1965) 1133–1138.
[19] Karlheinz Schwarz, Peter Blaha, Solid-state calculations using WIEN2k, Comput. Mater. Sci. 28 (2003) 259–273.
[20] Peter Blaha, Karlheinz Schwarz, Fabien Tran, Robert Laskowski, Georg K. H. Madsen, Laurence D. Marks, WIEN2k: an APW+lo program for calculating the properties of solids, J. Chem. Phys. 152 (2020), 074101.
[21] N.N. Anua, R. Ahmed, A. Shaari, M.A. Saeed, B.U. Haq, S. Goumri-Said, Non-local exchange correlation functionals impact on the structural, electronic and optical properties of III–V arsenides, Semicond. Sci. Technol. 28 (2013), 105015.
[22] H. Bennacer, A. Boukortt, S. Meskine, M. Hadjab, M.I. Ziane, A. Zaoui, First principles investigation of optoelectronic properties of $ZnXP_2$ (X = Si, Ge) lattice matched with silicon for tandem solar cells applications using the mBJ exchange potential, Optik 159 (2018) 229–244.
[23] M. Hadjab, S. Berrah, H. Abid, M.I. Ziane, H. Bennacer, B.G. Yalcin, Full-potential calculations of structural and optoelectronic properties of cubic indium gallium arsenide semiconductor alloys, Optik 127 (20) (2016) 9280–9294.
[24] M.B. Kanoun, S. Goumri-Said, A.E. Merad, J. Cibert, First-principles investigation of electronic structure and magnetic properties in ferromagnetic $Ga_{1-x}Mn_xN$ and $Al_{1-x}Mn_x$, J. Phys. D: Appl. Phys. 38 (2005) 1853.
[25] J.P. Perdew, A. Ruzsinszky, G.I. Csonka, O.A. Vydrov, G.E. Scuseria, L. A. Constantin, X. Zhou, K. Burke, Restoring the density-gradient expansion for exchange in solids and surfaces, PRL 100 (2008), 136406.
[26] A. Nagaoka, K. Yoshino, H. Taniguchi, T. Taniyama, K. Kakimoto, H. Miyake, Growth and characterization of $Cu_2ZnSn(S_xSe_{1-x})_4$ alloys grown by the melting method, J. Cryst. Growth 386 (2014) 204–207.
[27] I.D. Olekseyuk, I.V. Dudchak, L.V. Piskach, Phase equilibria in the Cu_2S–ZnS–SnS_2 system, J. Alloy. Compd. 368 (2004) 135–143.
[28] D. Fritsch, Revisiting the Cu-Zn disorder in kesterite type $Cu_2ZnSnSe_4$ employing a novel approach to hybrid functional calculations, Appl. Sci. 12 (2022) 2576.
[29] M.I. Ziane, D. Ouadjaout, M. Tablaoui, R. Nouri, W. Zermane, A. Djelloul, H. Bennacer, A. Mokrani, M. Hadjab, H. Abid, First-principle computed structural and thermodynamic properties of $Cu_2ZnSn(SxSe_{1-x})4$ pentanary solid solution, J. Electron Mater. 48 (2019) 6991–7002.
[30] M. Gusain, P. Rawat, R. Nagarajan, Solvent mediated rapid synthesis of orthorhombic Cu_2ZnSnS_4 (CZTS), Mater. Lett. 133 (2014) 220–223.
[31] Z. Yifen, L. Decong, L. Zuming, Phase transitions and electronic properties for zincblende-derived and wurtzite-derived stannite Cu_2ZnSnS_4 under pressure, J. Electron Mater. 46 (2017) 2812–2821.
[32] L. Guen, W.S. Glaunsinger, A. Wold, Physical properties of the quarternary chalcogenides $Cu2^IB^{II}C^{IV}X_4$ (B^{II} = Zn, Mn, Fe, Co; C^{IV} = Si, Ge, Sn; X = S, Se), Mat. Res. Bull. 14 (1979) 463–467.
[33] K. Doverspike, R. Kershaw, K. Dwight, A. Mold, Preparation and properties of the system $Cu_2Zn_{1-x}Fe_xGeS_4$, Mat. Res Bull. 23 (1988) 959–964.
[34] J. Chen, L. Zhao, F. Liu, S. Huang, Preparation and characterization of Cu_2ZnGeS_4 thin films by sulfurizing reactively sputtered precursors, in: L. Faraone, M. Martyniuk (Eds.), Proceedings of the Conf. Optoelectronic and Microelectronic Materials and Devices, IEEE, 2014, pp. 254–257.
[35] S. Levcenco, D. Dumcenco, Y.S. Huang, K.K. Tiong, C.H. Du, Anisotropy of the spectroscopy properties of the wurtz-stannite Cu_2ZnGeS_4 single crystals, Opt. Mater. 34 (2011) 183–188.
[36] K. Momma, F. Izumi, VESTA3 for three-dimensional visualization of crystal, volumetric and morphology data, J. Appl. Cryst. 44 (2011) 1272–1276.
[37] Q. Shu, J.-H. Yang, S. Chen, B. Huang, H. Xiang, X.-G. Gong, S.-H. Wei, $Cu_2Zn(Sn, Ge)Se_4$ and $Cu_2Zn(Sn,Si)Se_4$ alloys as photovoltaic materials: structural and electronic properties, Phys. Rev. B 87 (2013), 115208.
[38] J.-C. Crivello, J.-M. Joubert, N. Sokolovska, Supervised deep learning prediction of the formation enthalpy of complex phases using a DFT database: the a-phase as an example, Comput. Mater. Sci. 201 (2022), 110864.
[39] H.Y. Bai, B.X. Liu, Construction of the gibbs free energy diagram and interpretation of phase evolution in the Ni-Mo system, Phys. Stat. Sol. 136 (a) (1993) 73.
[40] T. Maeda, S. Nakamura, T. Wada, Phase stability and electronic structure of In-free photovoltaic semiconductors, $Cu_2ZnSnSe_4$ and Cu_2ZnSnS_4 by first-principles calculation, Mater. Res. Soc. Symp. Proc. (2009) 1165.
[41] L. Rycerz, J. Kapala, M. Gaune-Escard, Experimental mixing enthalpy and thermodynamic modelling of UCl_3-KCl, Syst. J. Mol. Liq. 342 (2021), 116963.

[42] A. Otero-de-la-Roza, D. Abbasi-Pérez, V. Luaña, Gibbs2: A new version of the quasiharmonic model code. II, Models Solid-State Thermodyn., Features Implement. Comput. Phys. Commun. 182 (11) (2011) 2232–2248.
[43] K. Doverspike, K. Dwight, A. Wold, Preparation and characterization of $Cu_2ZnGeS_{4-y}Se_y$, Chem. Mater. 2 (2) (1990) 194–197.
[44] N. Saini, J.K. Larsen, K.V. Sopiha, J. Keller, N. Ross, C. Platzer-Björkman, Germanium incorporation in Cu_2ZnSnS_4 and formation of a Sn Ge gradient, Phys. Status Solidi (a) Appl. Mater. Sci. 216 (19) (2019) 1900492.
[45] D.B. Khadka, J. Kim, Band gap engineering of alloyed $Cu_2ZnGe_xSn1–xQ4$ (Q=S, Se) films for solar cell, J. Phys. Chem. C. 119 (4) (2015) colcccc.